13th World Conference on Earthquake Engineering
Vancouver, B.C., Canada
August 1-6, 2004
Paper No. 2072

RISK ANALYSIS OF INDUSTRIAL STRUCTURES WITH HAZARDOUS MATERIALS UNDER SEISMIC INPUT

D.G. Talaslidis[1*], G.D. Manolis[1], E.A. Paraskevopoulos[2] and C.G. Panagiotopoulos[2]

SUMMARY

In this work, a methodology is presented for assessing seismic risk in industrial structures storing potentially hazardous chemicals. The components of a modular analysis software package specifically developed for this purpose are as follows: (a) Description of the seismic loading using synthetic accelerograms generated for various levels of peak ground acceleration (PGA) as white noise is filtered through layered soil; (b) Development of a finite element method (FEM) representation of the storage tank; (c) Derivation of a multi-degree-of-freedom (MDOF) stick model, which is based on matching key dynamic properties with those of the FEM model. In all cases, material non-linearities are taken into account; (d) Introduction of soil-structure-interaction (SSI) effects between tank and supporting ground; (e) Use of the Latin hypercube sampling method for probabilistic analyses of the structural system, whose stochastic parameters are the modulus of elasticity, the hardening parameter and the yield strength and (e) Generation of fragility curves for estimation of structural damage levels as functions of load intensity. The results generated herein are of interest in practical engineering design of industrial structures that pose a hazard in seismically prone regions.

1. INTRODUCTION

The development of methods for risk analysis based on probabilistic concepts in the presence of seismicity is a prerequisite for damage assessment in key structures (storage tanks, piping systems, industrial buildings, etc.) that comprise large industrial complexes [1,2]. Current design codes and guidelines cannot completely cover such issues, since much uncertainty is involved, primarily with respect to the nature of the various accident scenarios that are possible [3,4]. Further investigations are therefore required in order to obtain results that can be used in formulating comprehensive intervention strategies. Since these structural units form an integral part of larger installations, improvement in safety helps ensure a reliable and continuous operation of the entire industrial complex [5]. Current methods of structural analysis that assume a deterministic environment selectively utilize part of all available information regarding loading,

[1]Professor, Department of Civil Engineering, Aristotle University, Thessaloniki, Greece
*E-mail: talaslid@civil.auth.gr
[2]Graduate Student

material parameters and structural configuration and are thus capable of producing only representative values for the structural response [6]. The introduction of probabilistic models, especially in the description of the structure itself, requires a different level of analysis in order to provide quantitative information on structural reliability and on risk of failure.

Recent work in this area includes use of extensive MCS for the seismic finite element analysis of nuclear reactor facilities under seismic loads, including SSI effects [7]. Uncertainty is assumed to exist in the free-field motion, the local site conditions and the structural parameters, which are modelled by uniform, Gaussian and log-normal distributions. These random processes are in turn represented by their respective Karhunen-Loeve expansions and results are cast in terms of probabilistic in-structure spectra. Next, the nonlinear stochastic dynamic analysis of an SSI system consisting of an oscillator plus foundation resting on a 2D soil deposit was performed using the FEM with MCS in order to determine risk of damage due to liquefaction under earthquakes [8]. Soil properties were measured from cone penetration tests from a real site and were found to match a beta-distribution. The seismic input was modelled as a non-stationary random process and the analysis results were presented in terms of fragility curves. Fragility curves have also been used in conjunction with bridges, and their computation is based on either standard time history analyses or on simplified methods such as the capacity spectrum approach, which is essentially a static nonlinear procedure. Specifically, ten nominally identical, but statistically different highway bridges were analysed under eighty records of ground motion histories for this purpose [9]. Also, the seismic behaviour of on-grade, steel liquid storage cylindrical tanks subjected to ground shaking hazard was examined and fragility curves were developed by analysing the reported performance of over four hundred such tanks under nine separate earthquake events [10]. Finally, more refined statistical sampling techniques such as the Latin hypercube method [11] have been recently introduced for generating variations of a typical configuration for stochastic FEM analysis purposes. These sampling procedures improve the statistical representation of stochastic design parameters as compared to standard MCS, and also help reduce spurious correlations in the processed data.

In this work, an integrated methodology is developed for assessing risk to a typical industrial structure (see Fig. 1) with respect to accident scenarios involving seismically induced ground motions. As far as the structural model is concerned, the starting point is nonlinear, transient FEM analysis of cylindrical, thin-walled shell structures. This implies use of efficient triangular and quadrilateral shell finite elements based on the generalized Hu-Washizu principle within the context of elastoplastic material response [12]. Based on the results of the 3D finite element analyses, a simplified model in the form of a MDOF continuous beam with variable thickness is developed for capturing all salient aspects of the tank's response. SSI effects are accounted for by introducing simplified, yet realistic soil impedance coefficients [13]. Next, this MDOF system with material, geometric and loading parameters that are stochastic variables is used for assessing risk in the presence of random loads [14]. In particular, the basic failure mode considered is material yielding with local buckling ignored. Furthermore, two basic limit states are distinguished, namely serviceability and ultimate strength. The final results of the risk analysis is generation of fragility curves plotting limit state probability as a function of PGA, which allow for an estimation of damage levels in the structure under investigation.

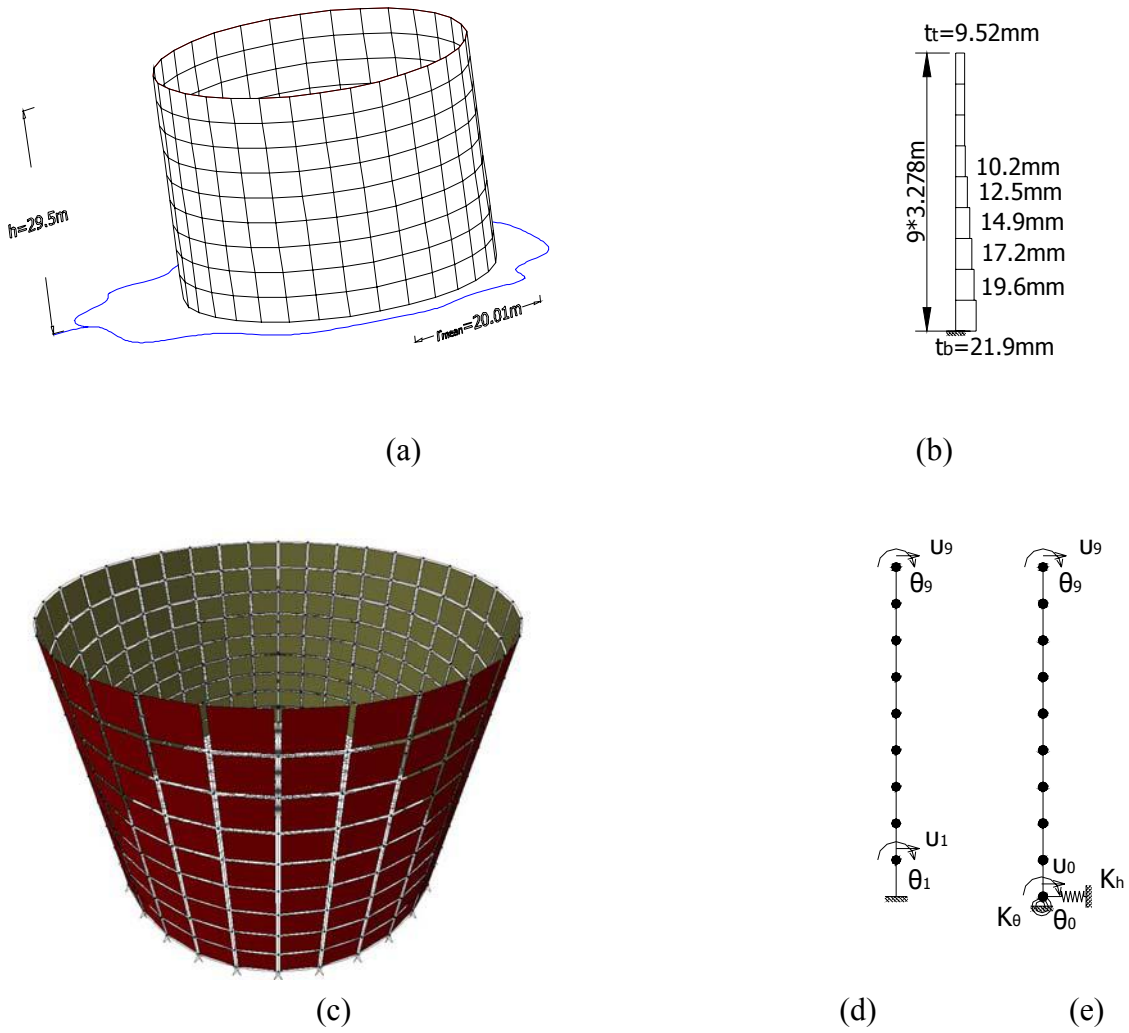

Figure 1: Steel storage tank: (a) geometry, (b) vertical cross-section, (c) finite element mesh, (d) equivalent MDOF model and (e) equivalent MDOF model with SSI.

2. SEISMIC LOAD DESCRIPTION

The simple, yet commonly used model of horizontally polarized, elastic shear (SH) waves is adopted herein. Soil layers over bedrock are modeled by the Kanai-Tajimi (KT) and by the high-pass (HP) filters in the frequency ω domain. Thus, the earthquake signal at the source is viewed as a broad-banded, white noise stochastic process with a constant power spectral density function (PSDF) S_0. This function is subsequently filtered through soil to yield the PSDF at the surface of the ground as

$$S_g(\omega) = H_k(\omega) H_h(\omega) S_0 \,,$$

$$H_k(\omega) = \left\{ 1 + 4\zeta_k^2 (\omega/\omega_k)^2 \right\} / \left\{ \left[1 - (\omega/\omega_k)^2 \right]^2 + 4\zeta_k^2 (\omega/\omega_k)^2 \right\} \text{ and} \qquad (1)$$

$$H_h(\omega) = (\omega/\omega_h)^2 / \left\{ \left[1 - (\omega/\omega_h)^2 \right]^2 + 4\zeta_h^2 (\omega/\omega_h)^2 \right\}$$

In the above, fundamental frequency ω_k and damping ratio ζ_k for the KT filter respectively range from 3π to 9π $(rad/\sec)$ and from 15% to 25% so as to cover a wide range of soil configurations. As far as the HP filter is concerned, these values are held fixed at $\omega_h = \pi$ $(rad/\sec)$ and at $\zeta_h = 100\%$.

In order to capture the uncertainty involved in ground seismicity, it is common to resort to MCS by considering certain parameters of the problem as random variables [15]. The most rational choice here is the PGA, which is a function of time t and of random parameter γ. A rather standard choice for the autocovariance of the PGA is the exponential correlation function, i.e.

$$\mathrm{cov}_g = <\ddot{x}_g(t,\gamma)^2> = \sigma_g^2 \exp(-\Delta t / t_g) f(t) \tag{2}$$

In the above, < > denotes the expectation operator for the ground accelerations $\ddot{x}_g(t)$, σ_g is their standard derivation, t_g is a correlation time interval, Δt is the time lapse and $f(t)$ is a deterministic time envelope. It is well known that the autocovariance and the PSDF form a Fourier transform pair so once the latter has been determined, it is possible to compute realizations of the PGA as

$$\ddot{x}_g(t) = \sqrt{2}\sum_{j=1}^{N} \sqrt{S_g(\omega_j)\Delta\omega}\cos\left(\omega_j t + \phi\right) f(t) \tag{3}$$

where $\Delta\omega = (\omega_2 - \omega_1)/N$ is the frequency increment and ϕ_j is a random phase angle uniformly distributed in the interval $[0, 2\pi]$. The frequency contents of the ground signal falls between cut-off frequencies $\omega_1 = 0.4\pi$ and $\omega_2 = 50\pi$ $(rad/\sec)$, while the envelope function shown below is essential in ameliorating the stationary assumption inherent in this simulation procedure:

$$f(t) = \begin{cases} (t/T_1)^2 & t \le T_1 \\ 1.0 & T_1 < t < T_2 \\ \exp\{-c(t-T_2)/T_D\} & t \ge T_2 \end{cases} \tag{4}$$

Rise and drop times respectively range as $T_1 = 1.0$ to $3.0\,\sec$ and $T_2 = 6.0$ to $8.0\,\sec$, while total signal duration is $T_D = 15.0$ (sec) and $c = 5$ is a dimensionless constant. Obviously, as the number of samples N in eqn (3) increases, the realizations become a more realistic representation of the original random field. Figure 2 summarizes the spatial and temporal distribution of the input to the tank from the ground motions. Finally, the Latin hypercube method will be used to produce a family of statistically equivalent acceleration records at a given PGA level, with the KT filter parameters and the envelope function characteristic times assumed to be random variables with uniform distributions. A total of six PGA levels that produce the full range of damage, from minor to severe, will be considered.

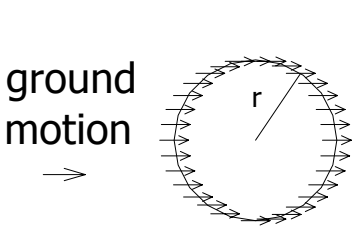

(a)

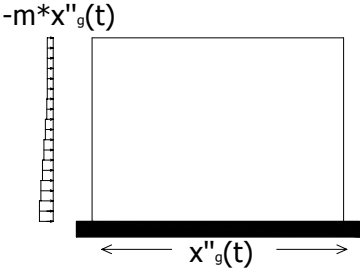

(b)

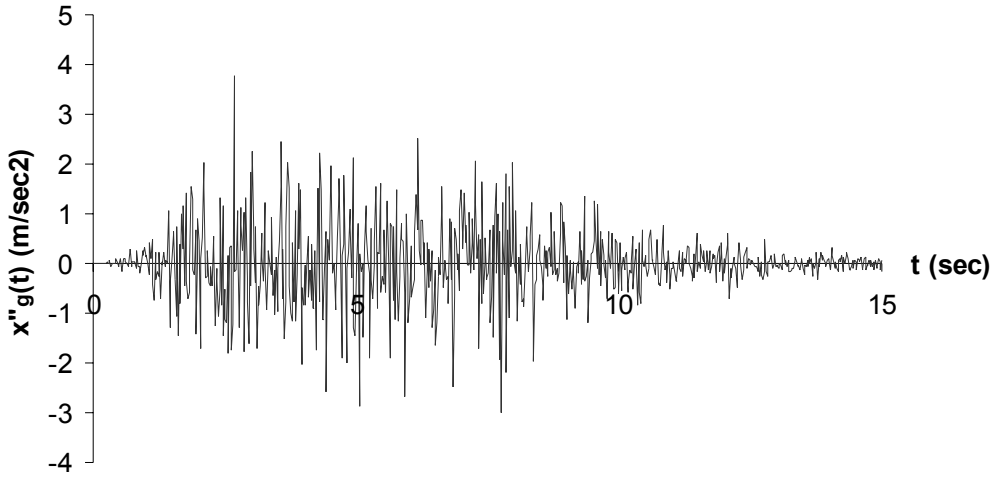

(c)

Figure 2: Seismic load: Spatial variation of the load (a) across the horizontal plane, (b) along the height and (c) spectrum-consistent synthetic ground acceleration history.

3. STRUCTURAL MODELS

The specific tank examined herein [16] has clear height $h = 29.5\ m$, mean base radius $r = 20.0\ m$ and its thickness t is variable, ranging from $t_b = 21.9\ mm$ at the base to $t_t = 9.52\ mm$ at the top (see in Fig. 1) There is a stiffener beam around the tank's perimeter at the top, while the tank's base is welded to a special metal alloy ring plate, which in turn rests on a concrete foundation. The tank material is ST 37 steel, with an elasticity modulus $E = 2.1 \times 10^8\ kN/m^2$, a Poisson's ratio $\nu = 0.30$ and a mass density $\rho = 7{,}850\ kg/m^3$. The plastic modulus is $E_{pl} = E \times 10^{-4}$, while the material yield stress is $\sigma_y = 2.35 \times 10^5\ kN/m^2$, and the yield strain and strain to fracture are $\varepsilon_y = 1.12\%$ and $\varepsilon_{ul} = 10.0\%$, respectively.

A FEM representation of the tank uses a simple, yet robust shell finite element [12] that was incorporated in an open-end computer program built around the facilities of commercial program Nastran [17]. Furthermore, the program employs Newmark's beta time integration algorithm, supplemented by the Newton-Raphson iterative scheme for capturing nonlinear response with the tangent modulus concept. Following standard convergence studies, the tank was modelled by 288 quadrilateral shell finite elements arranged in nine circumferential bands so as to account for variable wall thickness and to capture bending distortions near the lower edge of the tank's wall. The resulting mesh is shown in Fig. 1(c), and a free-vibration analysis was carried out. Firstly, the dominant eigenmode was identified, which is a symmetric, combined flexural-distortional mode at an eigenfrequency $f = 2.21 Hz$. When modal analysis was specified however, the resulting participation factor for this mode was very low (less than $\gamma = 0.01$). Therefore, another eigenmode with the largest participation factor for the forcing function vector particular to ground motions had to be identified, which turned out to be the skew-symmetric, bending mode at $f = 19.99\ Hz$ given in Fig. 3. The two participation factors for the seismic load, one for the

restoring forces ('static') and another for the inertia forces ('dynamic'), were $\gamma_{st} = 0.773$ and $\gamma_{dyn} = 0.486$, respectively.

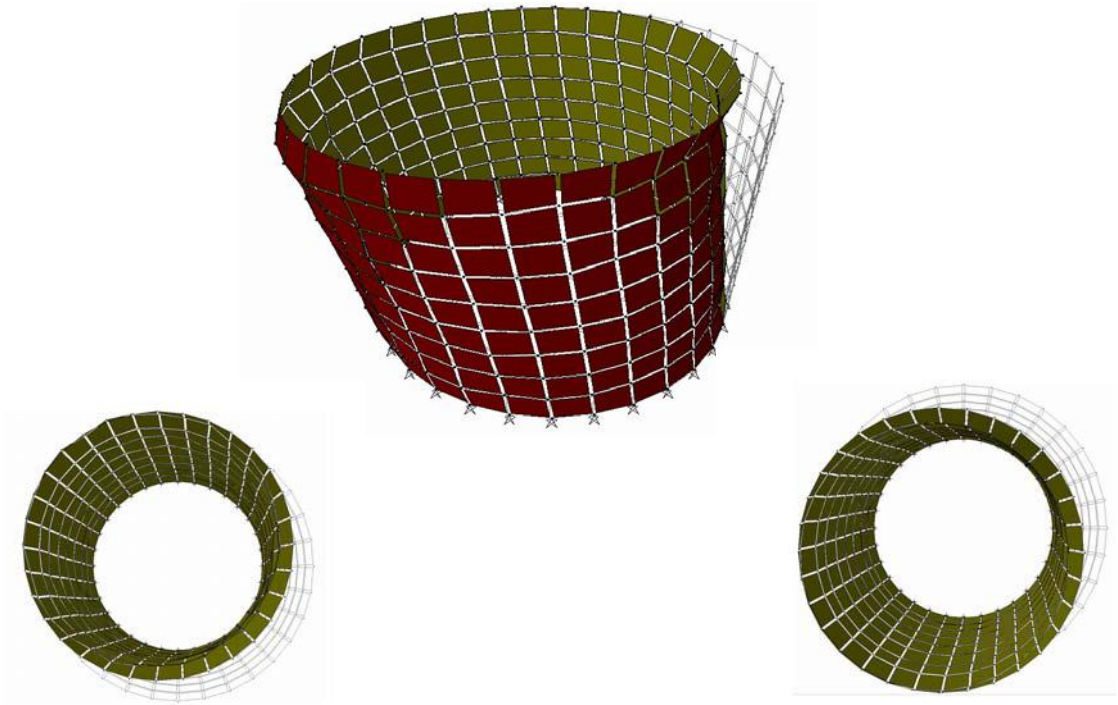

Figure 3: FEM modal analysis of the steel tank: Non-symmetric bending mode at $f = 19.99 Hz$ with the highest participation factor for the transient seismic load.

Based on the results of the eigenvalue analysis, a continuous, cantilevered beam model (see Fig. 1(d)) was developed for the steel tank. Firstly, the bending stiffness coefficients were computed by assuming a step-wise variable thickness with unit value at the bottom and by retaining the same thickness ratios of the original structure, which had nine circumferential bands of constant thickness decreasing from bottom to top. The height of the beam is the same as that of the original tank. Next, masses were lumped at the nine levels that demark change in thickness, and full fixity was assumed at the base. The value of the mass coefficient at the top node was adjusted so as to produce the fundamental frequency of $f = 19.99\ Hz$ associated with the dominant mode, and the remaining masses were adjusted by using the actual thickness ratios. Finally, a nominal amount of modal damping of 4.5% was prescribed, which is representative of rather flexible steel structures. Thus, a nine-node model was established with two DOF per node (translational and rotational) for a total of 18 active DOF, compared with the 320 DOF of the original 3D FEM model. As far as the loading sequence on this particular MDOF model is concerned, we use a step-wise uniform load whose value at the top is $p_{eq} = -m_{(level=9)}\, \ddot{x}_g$, while the variation of p_{eq} with height follows the thickness ratio of the original tank. The time variation of the synthetic ground accelerations remains unchanged.

The last task that remains is to adjust the material parameters of the MDOF model for the purposes of a nonlinear time-stepping analysis. To this purpose, a quasi-static ('push-over') analysis of the 3D FEM model is first performed for a step-wise uniformly distributed load across the height of the tank. The

constitutive law used derives from the bilinear, strain-hardening model for ductile steel, whose values were prescribed earlier on. At each load increment, the total base shear V_b in the FEM model is computed, normalized by the tank's total mass M, and plotted in Fig. 4 versus maximum lateral deflection u_t at the tank's top. The process is repeated until complete yielding of the base is reached. By curve-fitting a bilinear plot to the $\lambda = V_b / M$ versus u_t curve, a yield displacement $u_y = 0.0492\,m$ can be identified. Next, the 'pseudo-acceleration' $\lambda_y = 559.8\,(m/\sec^2)$ value that corresponds to u_y is converted into a load through multiplication by the tank mass at each level, scaled by the total tank to MDOF model mass ratio (about 30:1), and applied to the beam as a distributed load. The moment computed at the base of the continuous beam is the plastic (or yield) moment M_p.

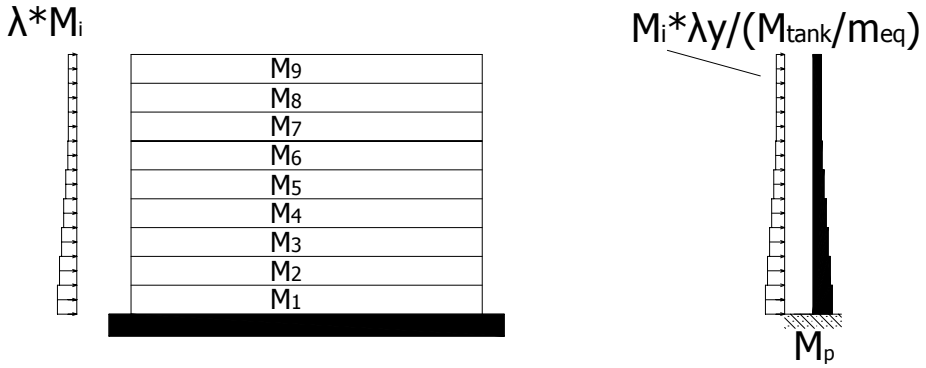

(a) (b)

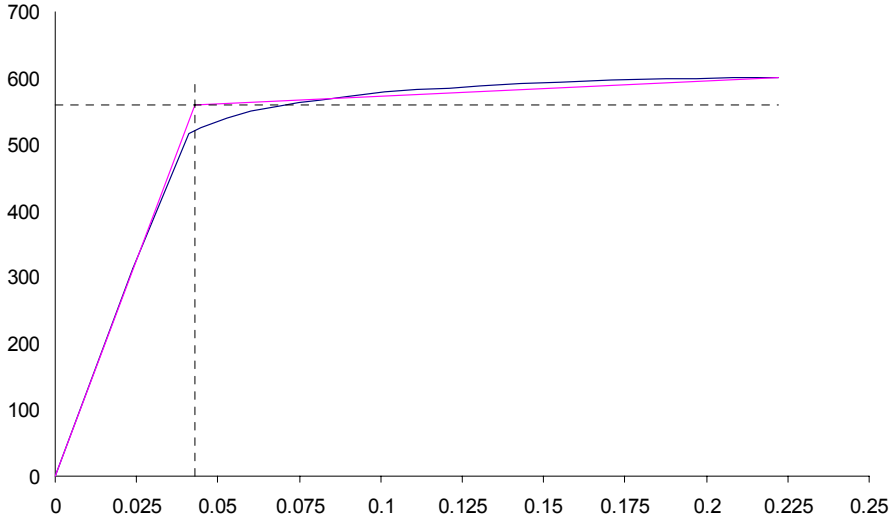

(c)

Figure 4: Nonlinear FEM analysis of the steel tank: (a) monotonically increasing lateral piece-wise uniform load, (b) normalized base shear versus top horizontal deflection curves and (c) computation of the plastic moment for the continuous beam model.

3.1 Equations of Motion

The MDOF model exhibiting elasto-plastic material behaviour that was calibrated above will now be incorporated within the context of an efficient probabilistic analysis for risk assessment. The basic parameters of this model are mass matrix $\boldsymbol{M}$, elastic tangent stiffness matrix $\boldsymbol{K}$, and damping matrix $\boldsymbol{C}$. In addition, it is necessary to introduce ductility μ as the ratio of maximum transient response to yield displacement u_y. The dynamic equilibrium equations of the MDOF structural system read as

$$\boldsymbol{M}\ddot{\mathbf{y}}(t) + \boldsymbol{C}\dot{\mathbf{y}}(t) + \boldsymbol{R}(t) = \boldsymbol{F}(t) \tag{5}$$

with $\boldsymbol{y}(t)$ denoting the vector of active DOF and $\boldsymbol{R}$ representing the restoring force vector. Specifically, in the elastic range, $\boldsymbol{R} = \mathbf{K}\,\boldsymbol{y}(t)$, while beyond it, the system is plastic with much reduced stiffness (the new coefficients are four orders of magnitude less than the elastic ones). Lastly, vector $\boldsymbol{F}(t)$ corresponds to external loads given by an inertia term $-\boldsymbol{M}\,\boldsymbol{I}\,\ddot{x}_g(t)$ applied along the height of the structure (where $\boldsymbol{I}^{\boldsymbol{T}} = [1,0,1,...,0]$) and the horizontal displacements $u_i(t)$ are defined as relative to the ground motion $x_g(t)$.

Equations (5) constitute an initial-value problem. The resulting system of nonlinear, second-order differential equations are numerically integrated by the generalized energy momentum algorithm [18]. This new algorithm adopts both linear and angular momentum conservation criteria during the current time step to avoid loss of unconditional stability that is commonly associated with elastic systems, along with desirable numerical dissipation characteristics. As an illustration of the type of results that were recovered, Fig. 5 shows the evolution of crown displacement $u_9(t)$ and base moment $M_b(t)$ for the empty steel tank with total mass $M = 403.34\,t$ (that corresponds to an equivalent MDOF model mass of $m_{eq} = 12.324\,t$), which is subjected to a synthetic earthquake acceleration record with PGA of $\ddot{x}_g = 0.38\,g$ and total duration $T_D = 15.0$ sec, which also corresponds to an intermediate load level of '4' (out of a scale ranging from '1-6'). A total of 750 time steps were used in the time integration algorithm and the criterion for yielding was $M_b(t) \geq M_p$. Note that plots for SSI effects, which will be discussed in the next section, are also included in the figure. It is interesting to note that a typical computer run for the MDOF model consumed a CPU time of less than 1.0 sec.

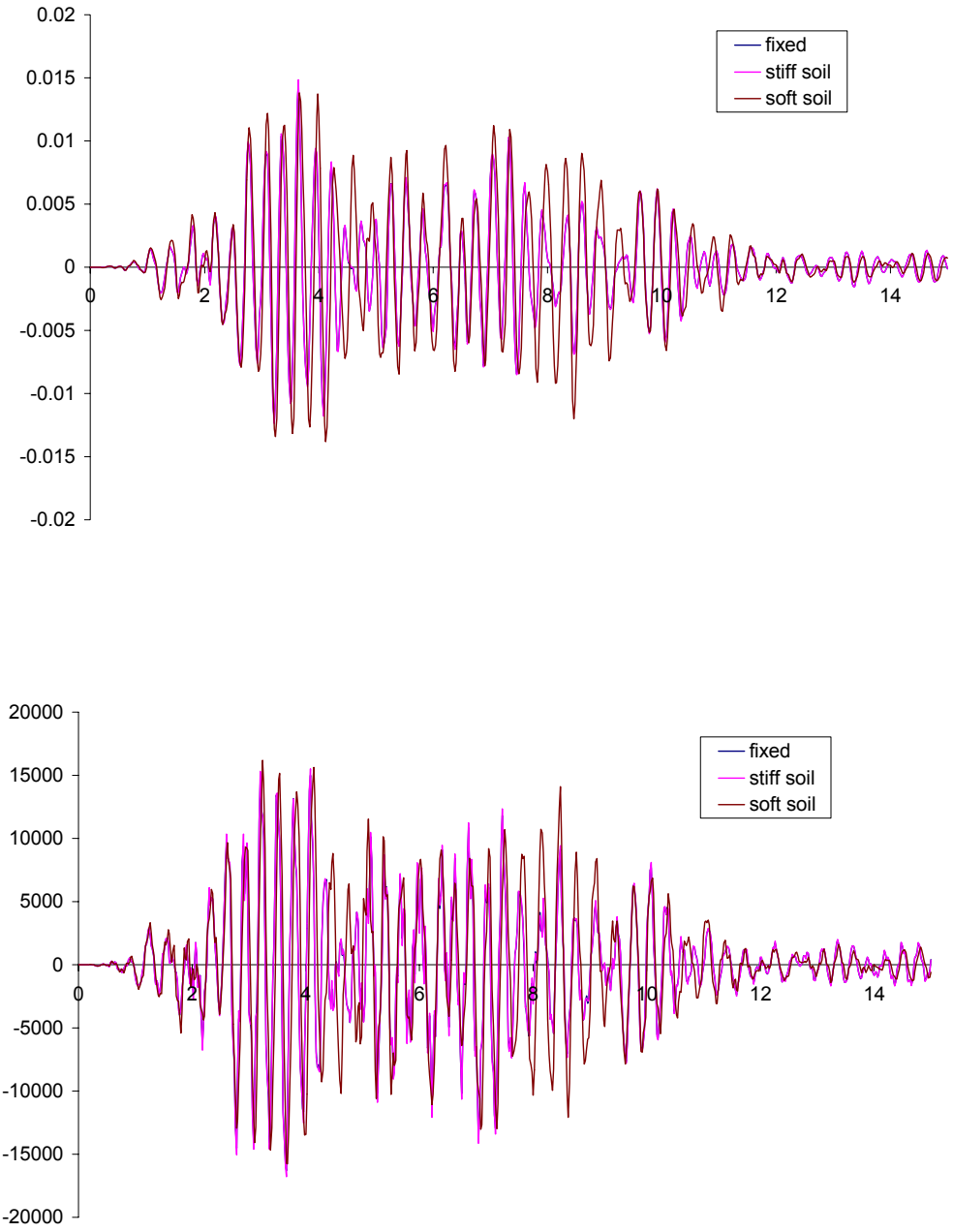

Figure 5: Time evolution of the MDOF steel tank response for seismic motions with PGA $\ddot{x}_g = 0.38\,g$: (a) top horizontal displacement u_9 and (b) base moment M_b.

3.2 Soil-Structure-Interaction Effects

SSI effects are manifested because of ground flexibility, in conjunction with the large mass (when the tank is full) and rather heavy foundation design of most cylindrical steel storage tanks. Since we seek the simplest model possible, a set of frequency-independent soil impedances, dampers and masses [13] were introduced, which for the case of a circular rigid foundation of radius r resting on ground are:

$$K_h = 8Gr/(2-\nu), \quad C_h = 1.08\sqrt{K_h \rho r^3}, \quad M_h = 0.28\rho r^3$$

$$K_\theta = 8Gr^3/\big(3(1-\nu)\big), \quad C_\theta = 0.47\sqrt{K_\theta \rho r^3}, \quad I_\theta = 0.49\rho r^5 \qquad (6)$$

In the above formulas, subscripts h, θ respectively denote horizontal and rotational DOF, as shown in Fig. 1(e). We assume relatively soft soil with the following numerical values for its properties: Poisson's ratio $\nu = 0.25$, shear modulus $G = 72.0 \cdot 10^6 \ kN/m^2$, density $\rho = 1{,}800 \ kg/m^3$ and shear wave-speed $c_s = \sqrt{(G/\rho)} = 200 \ m/\sec$. Basically, the influence of soil on the response of the overlying structure is elongation of the fundamental period of vibration, an effect that becomes more pronounced as the ratio of stiffness of structure to that of soil increases. SSI is not necessarily detrimental and, in fact, may lead to stress reduction in the structure at the expense of a more pronounced kinematic state. For stochastic loads, it usually leads an increase in the probability for a certain type of damage to occur at a given load level [14].

Thus, the additional equations of dynamic equilibrium for the horizontal displacement u_0 and angle of rotation θ_0 at the foundation (level *0*) are added to eqn (5) as follows:

$$\left[\begin{array}{c|cc} \mathbf{M} & & \\ \hline & M_h & 0 \\ & 0 & I_\theta \end{array}\right] \left\{\begin{array}{c} \ddot{\mathbf{y}} \\ \hline \ddot{u}_0 \\ \ddot{\theta}_0 \end{array}\right\} + \left[\begin{array}{c|cc} \mathbf{C} & & \\ \hline & C_h & 0 \\ & 0 & C_\theta \end{array}\right] \left\{\begin{array}{c} \dot{\mathbf{y}} \\ \hline \dot{u}_0 \\ \dot{\theta}_0 \end{array}\right\} + \left[\begin{array}{c|cc} \mathbf{K} & & \\ \hline & K_h & 0 \\ & 0 & K_\theta \end{array}\right] \left\{\begin{array}{c} \mathbf{y} \\ \hline u_0 \\ \theta_0 \end{array}\right\} = \left\{\begin{array}{c} \mathbf{F}(t) \\ \hline F_0 \\ 0 \end{array}\right\} \qquad (7)$$

The above is now a 20 DOF system, where I_θ is the mass moment of inertia corresponding to lumped mass M_h. Numerical results from computations involving the MDOF system with SSI are also plotted in Fig. 5. Two types of soil are considered whose lateral stiffness varies by two orders of magnitude, namely the soft soil given above (with $K_h = 2.1 \cdot 10^9 \ kN/m$) and a stiff soil (with $K_h = 210 \cdot 10^9 \ kN/m$). Comparisons show that the presence of SSI is of minor importance for such a flexible structure under relatively slowly developing motions, since all three curves (fixed, soft soil, stiff soil) are close together through-out the time duration of the ground accelerations. This however, may not be the case for other types of environmentally-induced loads [14].

4. RISK ANALYSIS

Risk is broadly defined as the convolution of hazard with consequence, i.e., the probability of occurrence of an event that can lead to failure times the loss associated with this event. Risk reduction is essentially a stochastic optimization problem [2], and additional aspects that should be considered is the influence of various structural components (sensitivity analysis), along with changes that can be implemented so as to reduce risk. On the hazard side of the equation, it is necessary to reduce existing failure probability, which is directly dependent on the randomness exhibited in the resistance of the structure as well as in the loading. In reliability analyses for non-linear systems, the capacity as well as the demand in conventional structures is usually assumed to be log-normally distributed [19].

4.1 Generation of Load and Structure Samples

Seismic Loads: These are characterized by the PGA output described in Section 2. At fixed PGA level, we discern a number of possible variations prior to activating the realizations given by eqs. (1)-(4) for producing synthetic accelerograms. These are produced by assuming the KT filter frequency ω_k and damping ζ_k , as well as time the envelope rise time T_1 , are all random variables with uniform distributions whose range is $(3\pi - 9\pi \; rad/\sec)$, $(0.15 - 0.25\ \%)$ and $(1.5 - 3.0 \ \sec)$, respectively. Next, we define six levels for the peak white noise intensity S_0 of the earthquake signal ranging from 0.005 to $0.0394 \; m^2/\sec^3$, in equal increments. These correspond to PGA levels of $0.15g$ to $0.45g$. Thus, at each PGA value, the synthetic ground motion family is matched with the structural model family of samples within the context of the Latin hypercube method and N pairs are solved, yielding an equal number of ductility values ì.

Structural Configuration: As far as the structural configuration is concerned, we consider certain key parameters to be random variables. These are the yield (or plastic) moment M_p whose mean value is $6{,}300 \; kN \cdot m$ and its standard deviation is $200 \; kN \cdot m$, the damping coefficient ζ ranging from $3\% - 6\%$, and the fluid mass M_{fl} stored in the tank. We assume the tank stores hydrocarbon fluids with mass density $\rho_{fl} = 0.5 \; kgr/m^3$, and the mean value corresponds to a half-empty configuration that gives $M_{fl} = 9{,}227 \; t$ (the equivalent MDOF model fluid mass is $m_{fl} = 300 \, t$). This fluid mass is lumped at the MDOF model node that is at a distance $h/3$ from the bottom of the tank. By prescribing a standard deviation of $50t$, the samples that will be generated cover the range from nearly empty to nearly full. Also, the bilinear elastoplastic material model uses an elastic bending stiffness of EI and a corresponding plastic stiffness $EI_{pl} = 10^{-4} EI$.

Structural Response: By specifying the above range and assuming a normal distribution for these parameters, the Latin hypercube method commences generation of a family of storage tanks. These tank samples are then matched with a family of seismic records. At this point, the minimum number of structure-load pairs (or samples) was taken as $N = 100$, following parametric studies in which the same results were recovered for larger values of N. Finally, the aforementioned six PGA levels were specified, which were gauged to produce structural behavior starting from mild elastic response up to pronounced nonlinearities. Thus, at each PGA level, N ductility values μ are obtained, which are statistically processed to yield the mean value m_L and second order reliability index β_L given in Table 1. We note here that this procedure was repeated with SSI effects included so as to capture the influence of ground flexibility on the ductility. This effect however turned out to be rather negligible (about $1\% - 2\%$ variation in both forces and displacements, for stiff as well as for soft soils).

Limit States: Next, five limit states are defined for the structure, as listed in Table 2. To each such state, the corresponding ductility capacity (or resistance factor R) is assumed to obey a logarithmic distribution with mean value $\mathrm{m_R}$ and second moment reliability index β_R. It should be noted here that the second order reliability index is equal to the logarithmic standard deviation of the structural capacity population (the same holds true for the structural response as well). It is subsequently used, along with the relevant mean value, to evaluate limit state probabilities.

Table 1: Logarithmic distribution of structural capacity (R) in terms of ductility.

Limit State	Mean Value m_R	Second moment reliability index β_R
Non-structural damage	1.0	0.5
Minor damage	2.0	0.5
Moderate damage	4.0	0.5
Severe damage	6.0	0.5
Collapse	7.5	0.5

Table 2: Logarithmic distribution of structural response (L) to seismic loads in terms of ductility.

Seismic Load Level	Mean Value m_L	Second moment reliability index β_L
1	0.1989	0.3680
2	0.2956	0.3460
3	0.3703	0.3847
4	0.4166	0.3506
5	0.4958	0.3704
6	0.5384	0.3558

4.2 Fragility Curves

The last step is to introduce the fragility of a structure with respect to a given limit state, which is defined as the probability P_f of load L exceeding resistance R and is given by

$$P_f = P(R \le L) = \int_0^\infty [1 - F_s(r)] f_R(r) dr \tag{8}$$

where F_s is the cumulative probability distribution of L and f_R is the probability density function of R. For both R and L log-normally distributed, eqn (8) can be written as

$$P_f = \Phi\left(-\ell n(m_R/m_L)\Big/\sqrt{\sigma_R^2 + \sigma_L^2}\right) \tag{9}$$

where Φ is the standardized normal distribution function. All results can now be summarized in the fragility curves of Fig. 6, which plot limit state damage probability P_f versus normalized PGA. We observe that for seismic loads, failure probability grows rather slowly with increasing PGA level, indicating that the flexible tank, whether full or empty, behaves rather well under slowly developing ground motions. It should be noted here that $P_f = 1.0$ denotes certain failure, which is never reached for this type of ground motions. Finally, SSI effects failed to produce any additional damage at a fixed level of intensity.

Based on these results, the following general conclusions can be drawn: (i) For every damage level, the probability that a certain structural configuration will exhibit the type of damage associated with it, increases with increasing load level; (ii) for every load level, the probability that a structure will exhibit damage greater than a certain predefined level decreases as the level of damage increases; (iii) the additional effect of foundation flexibility does not influence the probability for a certain damage level to

occur at fixed load intensity and (iv) seismic loads seem to have an overall mild effect on such a flexible structure, especially when the mass of the stored fluid is low.

$$P_f = P(R \leq L)$$

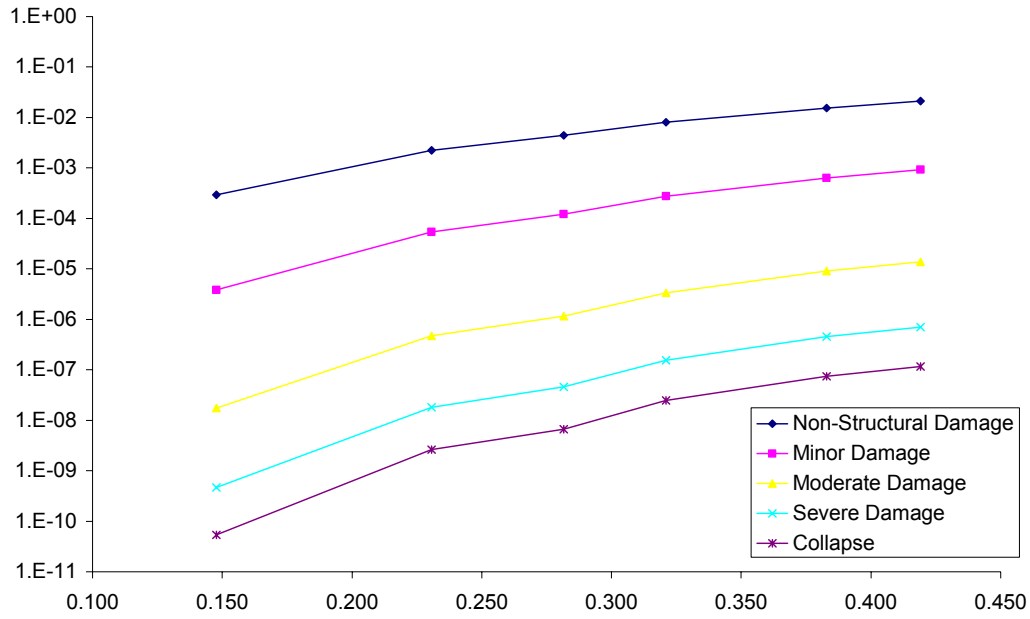

Figure 6: Fragility curves for a steel storage tank under seismically-induced ground motions.

5. CONCLUSIONS

An integrated numerical approach has been developed for assessing risk posed by earthquake motions to typical industrial structures. The analysis yields, as a final product, a set of fragility curves that allow computation of failure probabilities for steel storage tanks as functions of PGA. These curves are useful within the context of planning prevention and intervention strategies for large industrial complexes, where the type and intensity of the external loads are key parameters in estimating the level of damage sustained by various structural units. In addition, the presence of compliant soil causes SSI that do not have an appreciable effect regarding probability for a certain damage level to occur at fixed load intensity. In closing, it should be noted that the present methodology is general enough to be used for other categories of structures, as well as other types of extreme environmental and man-induced loads.

ACKNOWLEDGEMENT

The authors wish to thank the Greek General Secretariat for Research and Technology for its financial support of the project No. 1573 entitled “Development of Methodologies for Evaluating Risk in Industrial Units due to Explosions”.

REFERENCES

1. Yao, J.T.P. Probabilistic methods for the evaluation of seismic damage of existing structures, *Soil Dynamics and Earthquake Engineering* 1982; **1**: 91-96.
2. Schueller, G.I. and Ang, A.H.S. Advances in structural reliability, *Nuclear Engineering and Design* 1992; 134: 121-140.
3. Wen, Y.K. Building reliability and code calibration, *Earthquake Spectra* 1995; **11**: 269-349.
4. Franchin, P., Lupoi, A. and Pinto, P.E. Methods for seismic risk analysis: State-of-the-art versus advanced state of practice, *Journal of Earthquake Engineering-Special Issue* 2002; **6**(1) 131-155.
5. Lindell, M.K. and Perry, R.W. Earthquake impacts and hazard adjustment by acutely hazardous materials facilities following the Northridge earthquake, *Earthquake Spectra* 1998; **14**: 285-299.
6. Schueller, G.I. (editor) *Structural Dynamics-Recent Advances*. Berlin: Springer-Verlag, 1991.
7. Ghiocel, D.M. and Ghanem, R.G. Stochastic finite element analysis of seismic soil-structure-interaction, *Journal of Engineering Mechanics of ASCE* 2002; **128**: 66-77.
8. Koutsourelakis, S., Prevost, J.H. and Deodatis, G. Risk assessment of an interacting structure-soil system due to liquefaction, *Earthquake Engineering and Structural Dynamics* 2002; **31**: 851-879.
9. Shinozuka, M., Feng, M.Q., Kim, H.K. and Kim, S.H. Nonlinear static procedure for fragility curve development, *Journal of Engineering Mechanics of ASCE* 2000; **126**: 1287-1295.
10. O'Rourke, M.J. and So, P. Seismic fragility curves for on-grade steel tanks, *Earthquake Spectra* 2000; **16**: 801-815.
11. Olsson, A.M.J. and Sandberg, G.E. Latin hypercube sampling for stochastic finite element analysis, *Journal of Engineering Mechanics of ASCE* 2002; **128**: 121-125.
12. Talaslidis D. and Wempner G. The linear isoparametric triangular element-Theory and application, *Computer Methods in Applied Mechanics and Engineering* 1993; **103**: 375-397.
13. Wolf J.P. *Foundation Vibration Analysis using Simple Physical Models*. Englewood Cliffs: Prentice Hall, 1994.
14. D.G. Talaslidis, G.D. Manolis, E. Paraskevopoulos, C. Panayiotopoulos, N. Pelekasis and J.A. Tsamopoulos, Risk Analysis of Industrial Structures under Extreme Transient Loads, *Soil Dynamics and Earthquake Engineering*, to appear in 2004.
15. Shinozuka, M., Deodatis, G. and Harada, T. Digital simulation of seismic ground motion. In: Lin, Y.K. (editor) *Stochastic Approaches in Earthquake Engineering*. Berlin: Springer-Verlag, 1987; 252-298.
16. Liebich, G. and Boehler, I. FE-Berechnungen als Entwurfsgrundlage von LNG-Lagertanks bei dynamischen Belastungen, in *Proceedings Finite Elemente in der Baupraxis*. Berlin: Ernst und Sohn, 1995; 531-540.
17. *MSC / Nastran*, *Version 70*. Los Angeles: MacNeal-Schwendler Corporation, 1997.
18. Kuhl, D. and Ramm, E. Constrained energy momentum algorithm and its application to nonlinear dynamics of shells, *Computational Methods in Applied Mechanics and Engineering* 1996; **136**: 293-317.
19. Hwang, H.H.M. and Jaw J.W. Probabilistic damage analysis of structures, *Journal of Structural Engineering of ASCE* 1990; **116**: 1992-2007.